WARWICK
THE UNIVERSITY OF WARWICK

Manuscript version: Author's Accepted Manuscript
The version presented in WRAP is the author's accepted manuscript and may differ from the published version or Version of Record.

Persistent WRAP URL:
http://wrap.warwick.ac.uk/115281

How to cite:
Please refer to published version for the most recent bibliographic citation information. If a published version is known of, the repository item page linked to above, will contain details on accessing it.

Copyright and reuse:
The Warwick Research Archive Portal (WRAP) makes this work by researchers of the University of Warwick available open access under the following conditions.

Copyright © and all moral rights to the version of the paper presented here belong to the individual author(s) and/or other copyright owners. To the extent reasonable and practicable the material made available in WRAP has been checked for eligibility before being made available.

Copies of full items can be used for personal research or study, educational, or not-for-profit purposes without prior permission or charge. Provided that the authors, title and full bibliographic details are credited, a hyperlink and/or URL is given for the original metadata page and the content is not changed in any way.

Publisher's statement:
Please refer to the repository item page, publisher's statement section, for further information.

For more information, please contact the WRAP Team at: wrap@warwick.ac.uk.

warwick.ac.uk/lib-publications

Accepted manuscript
doi: 10.1680/jenge.18.00081

Accepted manuscript

As a service to our authors and readers, we are putting peer-reviewed accepted manuscripts (AM) online, in the Ahead of Print section of each journal web page, shortly after acceptance.

Disclaimer

The AM is yet to be copyedited and formatted in journal house style but can still be read and referenced by quoting its unique reference number, the digital object identifier (DOI). Once the AM has been typeset, an 'uncorrected proof' PDF will replace the 'accepted manuscript' PDF. These formatted articles may still be corrected by the authors. During the Production process, errors may be discovered which could affect the content, and all legal disclaimers that apply to the journal relate to these versions also.

Version of record

The final edited article will be published in PDF and HTML and will contain all author corrections and is considered the version of record. Authors wishing to reference an article published Ahead of Print should quote its DOI. When an issue becomes available, queuing Ahead of Print articles will move to that issue's Table of Contents. When the article is published in a journal issue, the full reference should be cited in addition to the DOI.

Downloaded by [UNIVERSITY OF WARWICK] on [19/03/19]. Copyright © ICE Publishing, all rights reserved.

Accepted manuscript
doi: 10.1680/jenge.18.00081

Submitted: 27 June 2018

Published online in 'accepted manuscript' format: 14 March 2019

Manuscript title: Morphological and Mineral Features of nZVI Induced Precipitation on Quartz Particles

Authors: Fuming Liu[1,2,3], Wan-Huan Zhou[1], Shuping Yi[3,4], Xueyu Geng[5]

Affiliations: [1]Department of Civil and Environmental Engineering, Faculty of Science and Technology, University of Macau, Macau, China. [2]Shenzhen Key Laboratory of Soil and Groundwater Pollution Control, Shenzhen, China. [3]School of Environmental Science and Engineering, Southern University of Science and Technology, Shenzhen, China. [4]Guangdong Provincial Key Laboratory of Soil and Groundwater Pollution Control, Shenzhen, China. [5]School of Engineering, The University of Warwick, Coventry, UK.

Corresponding author: Shuping Yi, School of Environmental Science and Engineering, Southern University of Science and Technology, Shenzhen, China. Tel.: 0755-88010147

E-mail: yisp@sustc.edu.cn

Downloaded by [UNIVERSITY OF WARWICK] on [19/03/19]. Copyright © ICE Publishing, all rights reserved.

Accepted manuscript
doi: 10.1680/jenge.18.00081

Abstract

Nano Zero-Valent Iron (nZVI) is a versatile nanomaterial that can not only efficiently remove contaminants in soil, but also improve the soil's geotechnical strength by changing their physicochemical properties. Inert solid mineral particles are the most common ingredients in soils, they present universal surface modification after the nZVI treatment. This study presents an investigation on the morphological and mineral features of nZVI induced iron mineral precipitations on quartz particles. Lead was employed as the artificial contaminant, while quartz was used to mimic the inert solid mineral particles in soil. Scanning Electron Microscope (SEM), Digital Image Analysis (DIA), Transmission Electron Microscopy (TEM), laser particle size analyzer, X-ray diffraction (XRD) and Raman spectrum were carried out for the characterization. The results indicate that iron minerals precipitated heterogeneously on the surface of quartz particles with plush-like and flake-like structure. They are made of deuterogenic plumbiferous minerals and ferriferous minerals. XRD analysis demonstrated that these minerals are amorphous. The curly flake-like mineral clusters were scatteredly distributed on the surface of quartz along with the of corroded nZVI aggregation. The thickness of the curly flake-like precipitation varied from 20 nm to 60 nm, and 20 nm to 35 nm for the plush-like precipitation. The generation of these iron mineral precipitations led to a slight increase in the average particle size and a decrease in the surface area of the soil. However, no clear difference in the shape and roughness of quartz was found after the nZVI treatment. This study is provided to improve the understanding of mass transfer from nZVI to inert solid particles in soil and its effect in soil improvement.

Downloaded by [UNIVERSITY OF WARWICK] on [19/03/19]. Copyright © ICE Publishing, all rights reserved.

Accepted manuscript
doi: 10.1680/jenge.18.00081

Introduction

Nano Zero-Valent Iron (nZVI) and the iron-mediated nanoparticles have high removal efficiency for various contaminants in soils, groundwater and wastewater. The target contaminants include these involved in pharmaceutical and personal care products (PPCP), halogenated organic compounds (HOCs), nitroaromatic compounds (NACs), arsenic, heavy metals, nitrate & phosphate, dyes and phenol (Lei et al., 2018; Stefaniuk et al., 2016). The chemical reaction of nZVI with these contaminants varies. In the aqueous system, redox reactions between nZVI and H_2O/O_2 spontaneously proceed as the following representative reactions (Liu et al., 2017):

$$Fe^o + 2H_2O \rightarrow Fe^{2+} + H_2 + 2OH^- \quad (1)$$

$$2Fe^o + O_2 + 2H_2O \rightarrow 2Fe^{2+} + 4OH^- \quad (2)$$

$$6Fe^{2+} + O_2 + 6H_2O \rightarrow 2Fe_3O_4(s) + 12H^+ \quad (3)$$

$$Fe^{2+} + 2OH^- \rightarrow Fe(OH)_2(s) \quad (4)$$

$$6Fe(OH)_2(s) + O_2 \rightarrow 2Fe_3O_4(s) + 6H_2O \quad (5)$$

The mechanisms of removal of contaminants using nZVI have been broadly investigated, in which a synergistic process of adsorption, reduction, oxidation, surface precipitation, surface complexation, and co-precipitation are generally involved (Zou et al., 2016). Additionally, the behavior of nZVI particles in environment and its resultant influence on the ecological system also have been extensively revealed. For instance, Adeleye found that the bulk of the nZVI injected into the polluted sites will end up in the sediment phase of the aquifer (Adeleye et al., 2013). They indicated that a loading level of iron higher than 500 g/kg may potentially affect

Downloaded by [UNIVERSITY OF WARWICK] on [19/03/19]. Copyright © ICE Publishing, all rights reserved.

Accepted manuscript
doi: 10.1680/jenge.18.00081

some organisms and also reduce the permeability of aquifers. A study conducted by Gil-Diaz et al. reported that the nZVI treatment stimulated the respiration and the dehydrogenase activity in soils, and no negative effects were found on the physicochemical and biological properties of soil (Fajardo et al., 2015; Gil-Diaz et al., 2014).

In view of the powerful redox reaction of nZVI, it is conceivable that the physicochemical properties of soil shall be changed, such as particle size, shape, roughness and mineral composition. This may subsequently lead to an alteration of soil's geotechnical properties over time (Keykha et al., 2015; Sreedeep S., 2015). Therefore, it is significant to investigate the effect of nZVI on the soil's geotechnical strength as it provides a crucial foundation for civil engineering. More attention should be paid to the potential changes of soil's geotechnical properties regarding the application of nZVI in the remediation of brownfield and the contaminated site in which soil will be reused as backfill. As a matter of fact, nZVI is such a utility nanomaterial that can not only efficiently remove contaminants in soil, but also improve the soil's mechanical strength. Nasehi et al. (2016) firstly demonstrated the effectiveness of nZVI in soil improvement and ascertained that the increased unconfined compressive strength (UCS) of the samples treated with nZVI was attributed to both colloidal reaction (cation exchange, flocculation, and agglomeration) and cementing reaction (pozzolanic reaction) among the particles of nZVI and the soil (Nasehi et al., 2016). However, their speculation is feeble because no clear evidence to support the colloidal reaction and cementing reaction.

Downloaded by [UNIVERSITY OF WARWICK] on [19/03/19]. Copyright © ICE Publishing, all rights reserved.

Accepted manuscript
doi: 10.1680/jenge.18.00081

Our previous study has demonstrated that the corrosion of nZVI and its induced precipitation is essentially evidence of the mass transfer from nZVI to the soil particles that responsible for the changes of physicochemical of soil and the improvement of soil's geotechnical strength (Zhou et al., 2018). However, soil particles composed predominantly of various minerals, organics, ions, and microorganisms etc. As the compositional complexity of soil, litter research clearly revealed the characteristic features of nZVI induced mass transformation as well as the precipitation on the soil particles.

Inert solid mineral particles (e. g. quartz, aluminum oxide, etc.) are the common components in soil and dominate the behavior of soil strength (Grytan et al., 2017; Kattidinesh et al., 2017). Endeavoring the clear characterization of the changes of morphological and mineral features of inert solid mineral particles in soil allows to make out the effect of nZVI treatment on the soil strength (Chinchu and Naidu, 2018; Habib-ur-Rehman et al. 2017). Quartz is one of the most common inert solid mineral constituents in soils. Because of its inherent chemical structure, quartz exists stably in soil and shows a very poor solubility (11.0 ± 1.1 mg/kg, at 25°C and 1 bar) (Martín-García et al., 2015). The oxidation reaction of nZVI with contaminated soil shall make a general difference on the inert solid mineral particles by changing their surface physicochemical properties. Therefore, a knowledge of the precipitation of nZVI induced precipitation on the quartz is of key importance to make out the heterogeneous reaction of nZVI in the soil system and its mechanism in soil improvement (Aldeeky et al., 2016; Nahar, 2018). To the best of our knowledge, few studies shed light onto this issue.

Downloaded by [UNIVERSITY OF WARWICK] on [19/03/19]. Copyright © ICE Publishing, all rights reserved.

Accepted manuscript
doi: 10.1680/jenge.18.00081

This study presents a characterization of nZVI induced iron mineral precipitations on quartz particles. It aims to detail the morphologic and mineral features of those precipitations on the inert solid particles in soil. Quartz (SiO_2) was used to simulate those inert solid particles in natural soil particle. Because using nZVI for stabilization of heavy metals has been investigated widely both in laboratory test and field remediation (Li et al., 2018), lead (Pb), a ubiquitous contaminant in soil, was used as the artificial contaminant for the premise of nZVI treatment. Specifically, Scanning Electron Microscope (SEM), Digital Image Analysis (DIA), Transmission Electron Microscopy (TEM), laser particle size analyzer, X-ray diffraction spectrum (XRD), and Raman spectrum were employed to evaluate the morphology and mineral features of the precipitation. The results of this study can improve the understanding of its derived bounding effects between nZVI and soil particles.

Methodology

Sample preparation

Chemical reagents ($Pb(NO_3)_2$, $FeCl_3 \cdot 6H_2O$ and $NaBH_4$) were of analytical grade and were used without further purification in the study. nZVI was prepared according to the suggestions reported by (Turabik and Simsek, 2017). In detail, 50 mL $NaBH_4$ solution (0.2 mol/L) was added dropwise into the 50 mL $FeCl_3 \cdot 6H_2O$ solution (0.05 mol/L) under the magnetic agitation of 500 rpm at the ambient temperature. The obtained dark sediment was wash using deionized water and ethanol for three times, respectively. After the air drying for 8 h at 35 ℃, the nZVI was obtained and sealed for usage.

Downloaded by [UNIVERSITY OF WARWICK] on [19/03/19]. Copyright © ICE Publishing, all rights reserved.

Accepted manuscript
doi: 10.1680/jenge.18.00081

To highlight the changes of physicochemical properties of quartz, four samples are prepared, namely pristine SiO_2, Pb-SiO_2, nZVI treated Pb-SiO_2, and nZVI-Pb sample: 1) Pristine SiO_2 was used to mimic inert solid particles in natural soil as received, without further processing. The others were prepared as follows: 2) Pb-SiO_2 sample: 30 mL deionized water, 6.4 mg $Pb(NO_3)_2$ and 10 g pristine SiO_2 were vividly mixed and aged for one week, then centrifuged and air dried at 35^oC for 24 hours. 4) nZVI treated Pb-SiO_2 sample: 30 mL deionized water, 6.4 mg $Pb(NO_3)_2$ and 10 g pristine SiO_2 were vividly mixed and aged for one week, followed by adding 1 g newly prepared nZVI and stirring evenly. The above mixture was then aged for one week, centrifuged and air dried at 35^oC for 24 hours. 4) nZVI-Pb sample: 1 g newly prepared nZVI was added into 30 mL 1000 ppm $Pb(NO_3)_2$ solution with mechanical agitation, aged for one week, then centrifuged and air dried at 35^oC for 24 hours. This sample was prepared to distinguish the mineral changes as a result of nZVI treatment.

Characterization

To characterize the morphologic features of the prepared samples, Scanning Electron Microscope (SEM), Digital Image Analysis (DIA), Transmission Electron Microscopy (TEM), and laser particle size analyzer were used. Scanning Electron Microscopy equipped with Energy Dispersive Spectrometer (SEM-EDS, Zeiss Merlin) was applied to depict the morphologic features and chemical composition. Digital image analysis of individual particles was analyzed using OCCHIO 500nano in water solution without agitation or ultrasound treatment, modified by the study reported by Sophie et al. (Leroy et al., 2011). A Hitachi HT7700 electron microscope with an accelerating voltage of 80 kV was used to conduct

Downloaded by [UNIVERSITY OF WARWICK] on [19/03/19]. Copyright © ICE Publishing, all rights reserved.

Accepted manuscript
doi: 10.1680/jenge.18.00081

Transmission Electron Microscopy (TEM) observations. Prior to the TEM test, ethyl alcohol was employed to disperse the simulated samples. Particle size distribution was characterized by a laser particle size analyzer (Malvern, Mastersizer 3000) in deionized water solution assisted with by the continuous electric mixing (3000 rpm) and ultrasound dispersion (40W, 40kHz).

The mineral texture of samples was evaluated using X-ray diffraction spectrum (XRD) and Raman spectrum. X-ray diffraction (XRD) was carried out at a scanning rate of 2.0°/min from 10° to 90° on Rigaku Smartlab (anode Cu, in configuration θ/2θ, with an acceleration tension of 45 kV and a current of 200 mA). Raman spectra was collected using a LabRam-1B (HORIBA, LabRAM HR Evolution) with a 532 nm He-Ne laser. Furthermore, approximately 1 mW of laser irradiation was used to stimulate the samples. Spectra were collected over the range 50-1000 cm^{-1}, averaging over 10 scans with individual exposure times of 10 seconds.

Result and discussion

The most pertinent physicochemical properties of a soil relevant to its strength are the morphological and mineral features of soil particles, particularly for those dominating inert solid particles. In this study, quartz is used to stimulate those inert solid particles in natural soil, with the aim to highlight the features of changes by the introduction of Pb and nZVI. SEM, Digital Image Analysis (DIA), TEM, and laser particle size analyzer were employed to evaluate the morphology features of samples. The shape of stimulated samples was firstly evaluated using SEM and Digital Image Analysis (DIA), as shown in Figures 1-3. The results indicated that the particle shape of pristine SiO_2 is irregular as other soil particles. The surface of quartz is relatively smooth with relative sharp edges. No obvious change of morphology

Downloaded by [UNIVERSITY OF WARWICK] on [19/03/19]. Copyright © ICE Publishing, all rights reserved.

Accepted manuscript
doi: 10.1680/jenge.18.00081

feature is distinguished in SEM images at a low-power field between the pristine SiO_2, Pb-SiO_2 sample, and nZVI treated Pb-SiO_2 sample (Figure 1). The results of Digital Image Analysis (DIA) presented a similar result, quartz particles in shapes were recorded (Figure 3). It is interesting that the roughness of Pb-SiO_2 remained almost identical after the nZVI treatment, as given by the digital images and calculated roughness value. The changeless shape of quartz can be ascribed to the following speculations: a) the particle spacing is relatively large as they were prepared without pre-consolidation; b) the solute of the Pb-SiO_2 is too simple. In other word, the roughness of soil particles may significantly change in practice considering the existence of various susceptive natural occurring organic matters, ions, and minerals that can be involved in the coprecipitation (Wen et al., 2014).

The morphology of the nZVI treated Pb-SiO_2 sample was further characterized using SEM at a high-power field, plush-like coating and curly flake-like mineral clusters are found on the surface of quartz (as shown in Figure 2). The curly flake-like mineral clusters principally appeared close to the corroded nZVI bulks. The chemical element analysis of the curly flake-like mineral clusters showed that they were composed primarily by Silicon (37.1%), Oxygen (49.9%), Iron (8.8%), and Lead (4.2%). These clusters are ascribed to the result of nZVI erosion by the restriction of metal iron growth in high precursor concentration (Hwang et al., 2011). Meanwhile, part of exchangeable Pb^{2+} are immobilized in the co-precipitation of ferrous and ferric ions. These two kinds of precipitations can be served as an evidence of mass transfer from nZVI to inert solid particles in soils, which is also consistent with the previous study reported by Arancibia-Miranda et al. (2014) (Arancibia-Miranda et al., 2014). The

Downloaded by [UNIVERSITY OF WARWICK] on [19/03/19]. Copyright © ICE Publishing, all rights reserved.

Accepted manuscript
doi: 10.1680/jenge.18.00081

aggregates of nZVI corrosion are distributed on the surface of quartz in a disorderly fashion. As a matter of fact, owning to the complexity of soil components, few studies have clearly presented this kind of morphologic features induced by nZVI treatment.

The single particle size of eroded nZVI particle is approximately 10 nm. Because of the aggregation phenomenon in the nZVI particles, the deuterogenic iron minerals are heterogeneously precipitated on the surface of quartz. The results of TEM images showed that the thickness of the plush-like coating on the surface of quartz varies from 20 nm to 35 nm, while the curly flake-like of that varies from 20 nm to 60 nm (Figure 4). The difference in their thickness is peculated to be related to the distance from the eroded nZVI aggregates.

The results of laser particle size analyzer are presented in Figure 5. It is showed that some quartz particles in larger size were generated after the Pb contamination. The generated quartz particles in larger size can hardly been found in SEM images. Meanwhile, a notable increase in the specific area of the quartz particles was presented after the introduction of Pb. This means that the introduction of Pb may result in a separation of smaller particles from the surface of a larger particle (Yukselen and Kaya, 2003). On the other hand, a slight increase of average particle size and a decrease of the specific area are recorded for the nZVI-treated sample. This increasing average particle size is presumably ascribed to the oxidation of nZVI aggregates, as well as its induced precipitation on the particles which bonding them together. Since no pre-consolidation was applied during the sample preparation, the bonding effects are faint but perceptible in the Digital Image Analysis (DIA).

Downloaded by [UNIVERSITY OF WARWICK] on [19/03/19]. Copyright © ICE Publishing, all rights reserved.

Accepted manuscript
doi: 10.1680/jenge.18.00081

X-ray diffraction (XRD) spectroscopy is used to examine the deuterogenic minerals after the immobilization of Pb by nZVI, as shown in Figure 6. The characteristic peaks of quartz (SiO_2, JCPDS No. 46-1045) are clearly presented in pristine SiO_2, Pb-SiO_2, and nZVI treated Pb-SiO_2 samples. However, no notable characteristic peak of deuterogenic plumbiferous mineral or ferriferous mineral crystals were found in Pb-SiO_2 and nZVI treated Pb-SiO_2 samples (Figure 6). This scenario suggests that those plush-like coating and protogenetic curly flake-like mineral clusters are found on the surface of quartz may be amorphous.

To further investigate the deuterogenic minerals observed in SEM and TEM images, sediment sample obtained from the oxidation of nZVI in Pb solution was prepared and characterised by XRD. Characteristic peaks of deuterogenic plumbiferous minerals including lead (Pb), massicot (PbO), and minium (Pb_3O_4), as well as ferriferous minerals including lepidocrocite (FeOOH), iron hydroxide oxide ($Fe(OH)_3$) and magnetite (Fe_3O_4) are presented in Table 2. The characteristic peaks of lead (Pb) are of higher intensity than that of massicot (PbO), and minium (Pb_3O_4). This indicates that predominantly adsorbing and reducing exchangeable Pb^{2+} to stable Pb^0 mechanisms were used to immobilize Pb^{2+} by nZVI (Wang et al., 2016). The lepidocrocite (FeOOH), iron hydroxide oxide ($Fe(OH)_3$) and magnetite (Fe_3O_4) minerals were generated by the oxidation of Fe^0 and precipitation of ferrous and ferric ions (Ruby et al., 2010, Kaze et al., 2017). However, no characteristic peak of Fe-Pb oxides or Fe^0 was observed. Since the nZVI were sufficient in the redox reaction, the deuterogenic massicot (PbO) and minium (Pb_3O_4) minerals generated slight oxidation and transformation of Pb^0 by water and oxygen during the drying procedure, of which nZVI were detached. When nZVI is

Downloaded by [UNIVERSITY OF WARWICK] on [19/03/19]. Copyright © ICE Publishing, all rights reserved.

Accepted manuscript
doi: 10.1680/jenge.18.00081

insufficient, exchangeable Pb^{2+} in an aqueous solution will be coprecipitated along with the precipitation of ferrous and ferric ions. This is then transformed into massicot (PbO) or minium (Pb_3O_4) minerals.

Raman spectroscopy is used in this study to further identify the deuterogenic compounds precipitated on the quartz that cannot easily be distinguished by XRD, as shown in Figure 7. There are ten clear bands at 127, 206, 264, 355, 392, 401, 465, 696, 806, 927 cm^{-1} – all of which are clearly observed in the Raman spectrum patterns of pristine SiO_2, Pb- SiO_2 and nZVI treated Pb-SiO_2. Slightly shift can be seen for the Pb-SiO_2 and nZVI treated Pb-SiO_2, revealing that the crystal lattice has been modified by the introduction of Pb ions. However, the bands of erosion products of iron oxides, such as lepidocrocite, iron hydroxide oxide, and magnetite, are clearly appeared in the nZVI treated SiO_2 and nZVI-Pb samples (Liu et al., 2015; Liu et al., 2017). Therefore, four bands at 68, 83, 138 and 215 cm^{-1} can be ascribed to lead oxide.

Based on the above analysis, a speculation is proposed that the nucleation in the crystal growth of the nZVI induced precipitation was impeded by the quartz particles, resulting the generation of these amorphous minerals heterogeneously precipitated on the surface of quartz particles. These minerals present different mineral characteristics when quartz was involved in the oxidation of nZVI. They may bond the soil particles together to form a firmer skeleton structure and improve the soil strength.

Conclusion

In this study, we have evaluated the morphology and mineral features of nZVI induced iron

Downloaded by [UNIVERSITY OF WARWICK] on [19/03/19]. Copyright © ICE Publishing, all rights reserved.

Accepted manuscript
doi: 10.1680/jenge.18.00081

mineral precipitation on the quartz particles, with the aim to improve the understanding of nZVI treatment in soil improvement. Lead was employed as an artificial contaminant for the premise of nZVI treatment, while quartz was used to imitate the inert solid mineral particles in soil. SEM-EDS, Digital Image Analysis (DIA), TEM, laser particle size analyzer, XRD, and Raman spectrum were involved for the evaluation.

The results indicate that corroded nZVI aggregations were dispersedly distributed on the surface of quartz after nZVI treatment. Two kinds of deuterogenic iron minerals shaped in plush-like coating and curly flake-like mineral clusters were found on the surface of quartz particles. The nucleation of the nZVI induced precipitation was presumably impeded by the quartz particles, which resulted in the amorphous structure of deuterogenic iron minerals. The XRD results of the sediment obtained from the oxidation of nZVI in Pb solution indicated that these precipitations are primarily made of lead (Pb), massicot (PbO), minium (Pb_3O_4), lepidocrocite (FeOOH), iron hydroxide oxide ($Fe(OH)_3$), and magnetite (Fe_3O_4). Part of exchangeable Pb^{2+} was immobilized by the co-precipitation of ferrous and ferric ions and incorporated into the iron mineral precipitations. The thickness of these mineral precipitation varied from 20 nm to 60 nm. The introduction of nZVI resulted in a slight increase of the average particle size and a decrease in the specific area of the soil. However, no clear difference in the shape and roughness of quartz was found after the nZVI treatment.

Because soils are generally made of motley minerals, ions, natural organic matters, and microorganisms, it is advised that more investigation should be carried out to study the behavior of various nanoparticles on the changes of physicochemical properties of individual

Downloaded by [UNIVERSITY OF WARWICK] on [19/03/19]. Copyright © ICE Publishing, all rights reserved.

Accepted manuscript
doi: 10.1680/jenge.18.00081

or combined substances in soil. Only after that can we achieve a more accurate cognition on the mechanism of nanoparticles in changing the soil's geotechnical properties such as these involved in undrained shear strength, cohesion, internal friction angle, and so on.

Acknowledgements

The authors wish to thank financial supports from the Macau Science and Technology Development Fund (FDCT) (Code: 125/2014/A3), the University of Macau Research Fund (MYRG2017-00198-FST), Shenzhen Peacock Plan (KQTD2016022619584022), Shenzhen basic research plan (JCYJ20160429191638556), Guangdong Provincial Key Laboratory of Soil and Groundwater Pollution Control (2017B030301012), and National Natural Science Foundation of China (1678319).

Downloaded by [UNIVERSITY OF WARWICK] on [19/03/19]. Copyright © ICE Publishing, all rights reserved.

Accepted manuscript
doi: 10.1680/jenge.18.00081

References

Adeleye A S, A A Keller, R J Miller and H S Lenihan (2013) Persistence of commercial nanoscaled zero-valent iron (nZVI) and by-products. Journal of Nanoparticle Research 15(1): 1418, https://doi.org/10.1007/s11051-013-1418-7

Aldeeky H, O Al Hattamleh and B Abu Alfoul (2016) Effect of sand placement method on the interface friction of sand and geotextile. International Journal of Civil Engineering 14(2): 133-138, https://doi.org/10.1007/s40999-016-0019-0

Arancibia-Miranda N, S E Baltazar, A Garcia, A H Romero, M A Rubio and D Altbir (2014) Lead removal by nano-scale zero valent iron: Surface analysis and pH effect. Materials Research Bulletin 59: 341-348, https://doi.org/10.1016/j.materresbull.2014.07.045

Chinchu C and A D Naidu (2018) Material characterisation by digital image analysis: a review. Environmental Geotechnics 5(5): 249-262, https://doi.org/10.1680/jenge.16.00010

Fajardo C, M Gil-Diaz, G Costa, J Alonso, A M Guerrero, M Nande, M C Lobo and M Martin (2015) Residual impact of aged nZVI on heavy metal-polluted soils. Science of the Total Environment 535: 79-84, https://doi.org/10.1016/j.scitotenv.2015.03.067

Gil-Diaz M M, A Perez-Sanz, M A Vicente and M C Lobo (2014) Immobilisation of Pb and Zn in soils using stabilised zero-valent iron nanoparticles: effects on soil properties. Clean-Soil Air Water 42(12): 1776-1784, https://doi.org/10.1002/clen.201300730

Grytan S, D Ashish and S Sumi (2017) Preparation of Wyoming bentonite nanoparticles. Environmental Geotechnics 4(5): 373-381, https://doi.org/10.1680/jenge.15.00001

Habib-ur-Rehman A and S N N Abduljauwadsahel (2017) Molecular-level simulations of

Downloaded by [UNIVERSITY OF WARWICK] on [19/03/19]. Copyright © ICE Publishing, all rights reserved.

Accepted manuscript
doi: 10.1680/jenge.18.00081

oil-contaminated clays. Environmental Geotechnics 0(0): 1-15, https://doi.org/10.1680/jenge.16.00032

Hwang Y H, D G Kim and H S Shin (2011) Effects of synthesis conditions on the characteristics and reactivity of nano scale zero valent iron. Applied Catalysis B: Environmental 105(1): 144-150, https://doi.org/10.1016/j.apcatb.2011.04.005

Kattidinesh R, R Patwaryzillur, S Kattikalpana (2017) Modelling clay–fluid interactions in montmorillonite clays. Environmental Geotechnics 4(5): 322-338, https://doi.org/10.1680/jenge.14.00027

Kaze R C, L M Beleuk à Moungam, M L Fonkwe Djouka, A Nana, E Kamseu, U F Chinje Melo and C Leonelli (2017) The corrosion of kaolinite by iron minerals and the effects on geopolymerization. Applied Clay Science 138: 48-62, https://doi.org/10.1016/j.clay.2016.12.040

Keykha H A, B B K Huat, A Asadi, M Zareian and S Kawasaki (2015) Electrokinetic properties of pasteurii and aquimarina bacteria. Environmental Geotechnics 2(3): 181-188, https://doi.org/10.1680/envgeo.13.00072

Lei C, Y Sun, D C W Tsang and D Lin (2018) Environmental transformations and ecological effects of iron-based nanoparticles. Environmental Pollution 232: 10-30, https://doi.org/10.1016/j.envpol.2017.09.052

Leroy S, G Dislaire, D Bastin and E Pirard (2011) Optical analysis of particle size and chromite liberation from pulp samples of a UG2 ore regrinding circuit. Minerals Engineering 24(12): 1340-1347, https://doi.org/10.1016/j.mineng.2011.06.006

Downloaded by [UNIVERSITY OF WARWICK] on [19/03/19]. Copyright © ICE Publishing, all rights reserved.

Accepted manuscript
doi: 10.1680/jenge.18.00081

Li Z, L Wang, J Meng, X Liu, J Xu, F Wang and P C Brookes (2018) Zeolite-supported nanoscale zero-valent iron: New findings on simultaneous adsorption of Cd(II), Pb(II), and As(III) in aqueous solution and soil. Journal of Hazardous Materials 344: 1-11, https://doi.org/10.1016/j.jhazmat.2017.09.036

Liu A, J Liu, J Han and W X Zhang (2017) Evolution of nanoscale zero-valent iron (nZVI) in water: Microscopic and spectroscopic evidence on the formation of nano- and micro-structured iron oxides. Journal of Hazardous Materials 322: 129-135, https://doi.org/10.1016/j.jhazmat.2015.12.070

Liu A R, J Liu and W X Zhang (2015) Transformation and composition evolution of nanoscale zero valent iron (nZVI) synthesized by borohydride reduction in static water. Chemosphere 119: 1068-1074, https://doi.org/10.1016/j.chemosphere.2014.09.026

Martín-García J M, R Márquez, G Delgado, M Sánchez-Marañón and R Delgado (2015) Relationships between quartz weathering and soil type (Entisol, Inceptisol and Alfisol) in Sierra Nevada (southeast Spain). European Journal of Soil Science 66(1): 179-193, https://doi.org/10.1111/ejss.12214

Nahar S S (2018). A review on mobility of engineered carbon-based nanoparticles in porous media. Environmental Geotechnics 0(0): 1-11, https://doi.org/10.1680/jenge.17.00002

Nasehi S A, A Uromeihy, M R Nikudel and A Morsali (2016) Use of nanoscale zero-valent iron and nanoscale hydrated lime to improve geotechnical properties of gas oil contaminated clay: a comparative study. Environmental Earth Sciences 75(9), https://doi.org/10.1007/s12665-016-5443-6

Downloaded by [UNIVERSITY OF WARWICK] on [19/03/19]. Copyright © ICE Publishing, all rights reserved.

Accepted manuscript
doi: 10.1680/jenge.18.00081

Ruby C, M Usman, S Naille, K Hanna, C Carteret, M Mullet, M François and M Abdelmoula (2010) Synthesis and transformation of iron-based layered double hydroxides. Applied Clay Science 48(1): 195-202, https://doi.org/10.1016/j.clay.2009.11.017

Sreedeep S (2015) Vision ahead for environmental geotechnics. Environmental Geotechnics 2(5): 255-256, https://doi.org/10.1680/envgeo.13.00101

Stefaniuk M, P Oleszczuk and Y S Ok (2016) Review on nano zerovalent iron (nZVI): From synthesis to environmental applications. Chemical Engineering Journal 287: 618-632, https://doi.org/10.1016/j.cej.2015.11.046

Turabik M and U B Simsek (2017) Effect of synthesis parameters on the particle size of the zero valent iron particles. Inorganic and Nano-Metal Chemistry 47(7): 1033-1043, https://doi.org/10.1080/15533174.2016.1219869

Wang W, Y L Hua, S L Li, W L Yan and W X Zhang (2016) Removal of Pb(II) and Zn(II) using lime and nanoscale zero-valent iron (nZVI): A comparative study. Chemical Engineering Journal 304: 79-88, https://doi.org/10.1016/j.cej.2016.06.069

Wen Z, Y Zhang and C Dai (2014) Removal of phosphate from aqueous solution using nanoscale zerovalent iron (nZVI). Colloids and Surfaces A: Physicochemical and Engineering Aspects 457: 433-440, https://doi.org/10.1016/j.colsurfa.2014.06.017

Yukselen Y and A Kaya (2003) Zeta Potential of kaolinite in the presence of alkali, alkaline earth and hydrolyzable metal ions. Water, Air, and Soil Pollution 145(1): 155-168, https://doi.org/10.1023/A:1023684213383

Zhou W H, F Liu, S Yi, Y Z Chen, X Geng and C Zheng (2018) Simultaneous stabilization of

Downloaded by [UNIVERSITY OF WARWICK] on [19/03/19]. Copyright © ICE Publishing, all rights reserved.

Accepted manuscript
doi: 10.1680/jenge.18.00081

Pb and improvement of soil strength using nZVI. Science of The Total Environment, https://doi.org/10.1016/j.scitotenv.2018.09.146

Zou Y D, X X Wang, A Khan, P Y Wang, Y H Liu, A Alsaedi, T Hayat and X K Wang (2016) Environmental remediation and application of nanoscale zero-valent iron and its composites for the removal of heavy metal ions: a review. Environmental Science & Technology 50(14): 7290-7304, https://doi.org/10.1021/acs.est.6b01897

Downloaded by [UNIVERSITY OF WARWICK] on [19/03/19]. Copyright © ICE Publishing, all rights reserved.

Accepted manuscript
doi: 10.1680/jenge.18.00081

Table 1. Physicochemical parameters of samples

Item [a]	SiO_2	Pb-SiO_2	nZVI treated Pb-SiO_2
Silicon (Si)	-	-	37.1
Oxygen (O)	-	-	49.9
Iron (Fe)	-	-	8.8
Lead (Pb)	-	-	4.2
D [4,3]/um [b]	30.7	30.4	46.7
Dv (50)/um [b]	21.1	18.6	29.1
Dv (90)/um [b]	73.7	118.0	109
Specific area/$m^2 \cdot Kg^{-1}$ [b]	994.5	1264	755.8
Roughness (90%) [c]	-	21.4	21.1

Note:

[a] analysis point of chemical element composition was obtained from EDS, as is shown in Figure 2;

[b] D [4,3], Dv (50), and Dv (90)/ were obtained from laser particle size analyzer;

[c] roughness (90%) was obtained from Digital Image Analysis (DIA) of individual particles using OCCHIO 500nano.

Downloaded by [UNIVERSITY OF WARWICK] on [19/03/19]. Copyright © ICE Publishing, all rights reserved.

Accepted manuscript
doi: 10.1680/jenge.18.00081

Table 2. Characteristic peaks of the deuterogenic ferriferous and plumbiferous mineral crystals

Mineral Crystal	Chemical Formula	JCPDS No.	Characteristic Peaks/2θ
Lead	Pb	04-0686	31.305°, 36.266°, 52.228°, 62.119°, 65.236°, 85.394°, 88.196°
Massicot	PbO	38-1477	15.017°, 22.110°, 29.078°, 30.315°, 36.066°, 52.304°, 85.087°
Minium	Pb_3O_4	76-1799	14.222°, 26.338°, 27.165°, 28.668°, 30.790°, 32.139°, 39.905°
Lepidocrocite	FeOOH	74-1877	14.147°, 26.072°, 30.009°, 36.387°, 46.866°, 55.823°, 62.425°
Iron Hydroxide Oxide	$Fe(OH)_3$	38-0032	14.188°, 21.223°, 36.373°, 38.049°, 46.865°, 60.197°, 80.922°
Magnetite	Fe_3O_4	77-1545	18.285°, 30.076°, 370.57°, 47.139°, 62.520°, 70.926°, 78.922°
Quartz	SiO_2	99-0088	20.809°, 26.640°, 36.546°, 39.467°, 40.291°, 50.140°, 59.960°

Downloaded by [UNIVERSITY OF WARWICK] on [19/03/19]. Copyright © ICE Publishing, all rights reserved.

Accepted manuscript
doi: 10.1680/jenge.18.00081

Figure 1. SEM images at a low-power field (Mag.= 1.00 KX): a) pristine SiO_2; b) Pb-SiO_2; c) nZVI treated Pb-SiO_2

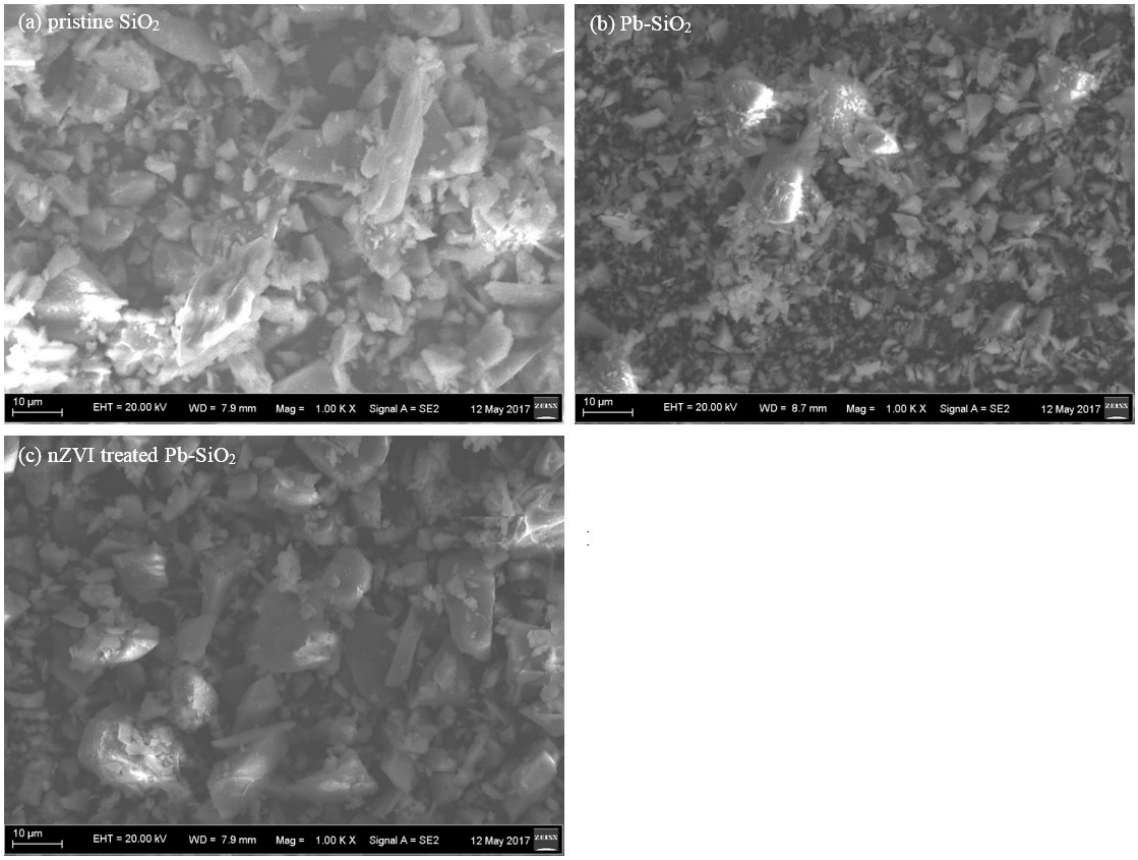

Downloaded by [UNIVERSITY OF WARWICK] on [19/03/19]. Copyright © ICE Publishing, all rights reserved.

Accepted manuscript
doi: 10.1680/jenge.18.00081

Figure 2. SEM images at a high-power field (Mag.= 23.34 KX and 3.97 KX): a) curly flake-like nZVI induced iron mineral precipitation on the surface of quartz; b) nZVI treated Pb-SiO_2; c) EDS result of curly flake-like nZVI induced iron mineral precipitation

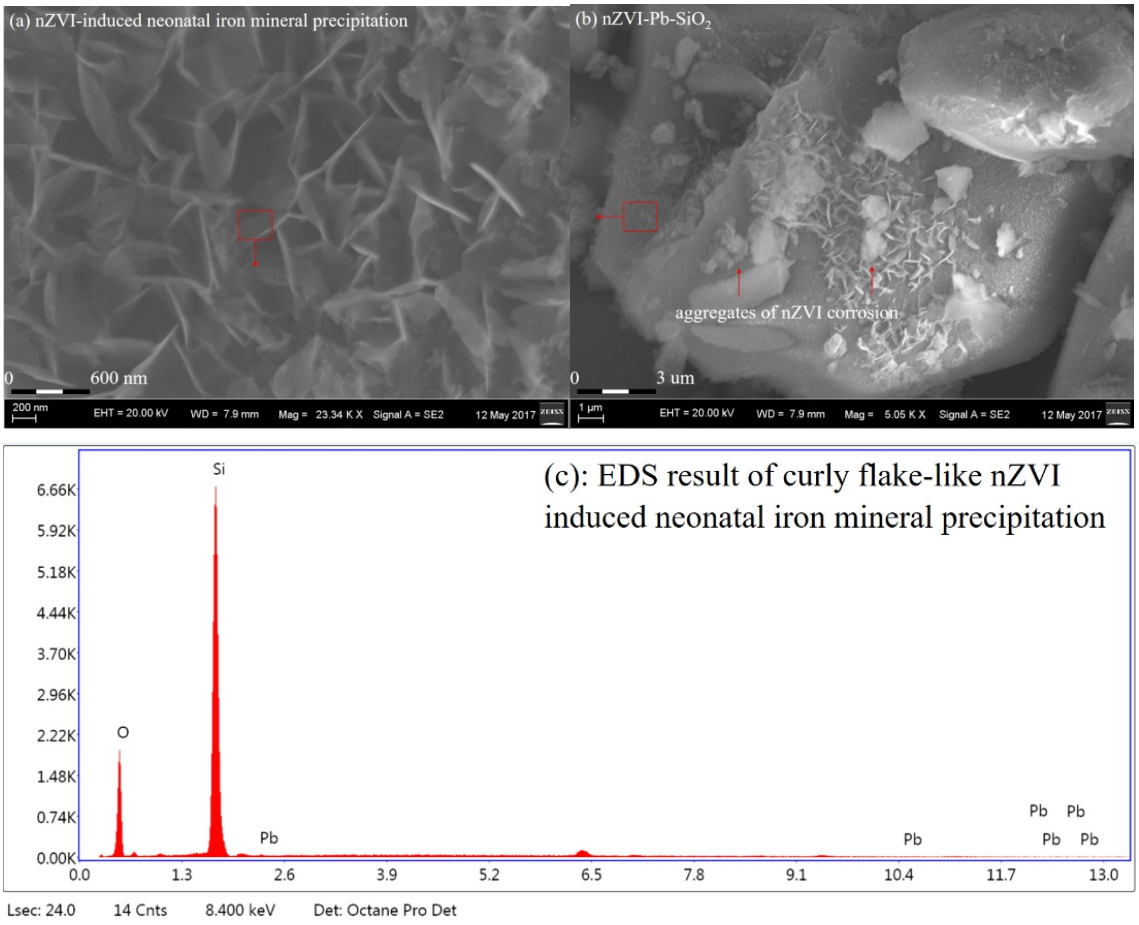

Downloaded by [UNIVERSITY OF WARWICK] on [19/03/19]. Copyright © ICE Publishing, all rights reserved.

Accepted manuscript
doi: 10.1680/jenge.18.00081

Figure 3. Typical shapes of individual quartz particle after the Pb contamination and nZVI treatment

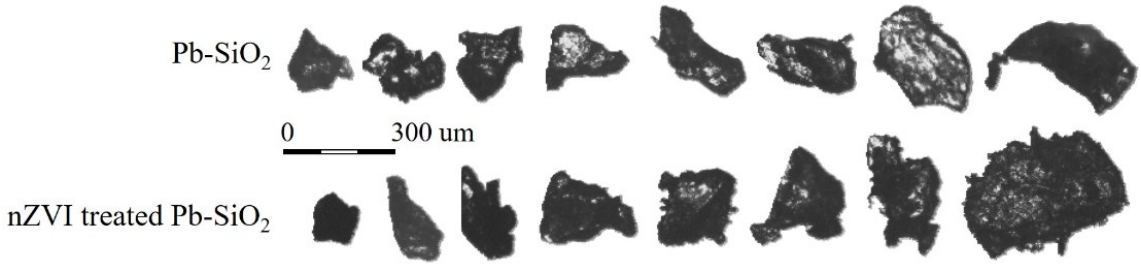

Downloaded by [UNIVERSITY OF WARWICK] on [19/03/19]. Copyright © ICE Publishing, all rights reserved.

Accepted manuscript
doi: 10.1680/jenge.18.00081

Figure 4. TEM images of nZVI induced iron mineral precipitation on the surface of quartz: a) curly flake-like precipitation; b) plush-like coating precipitation

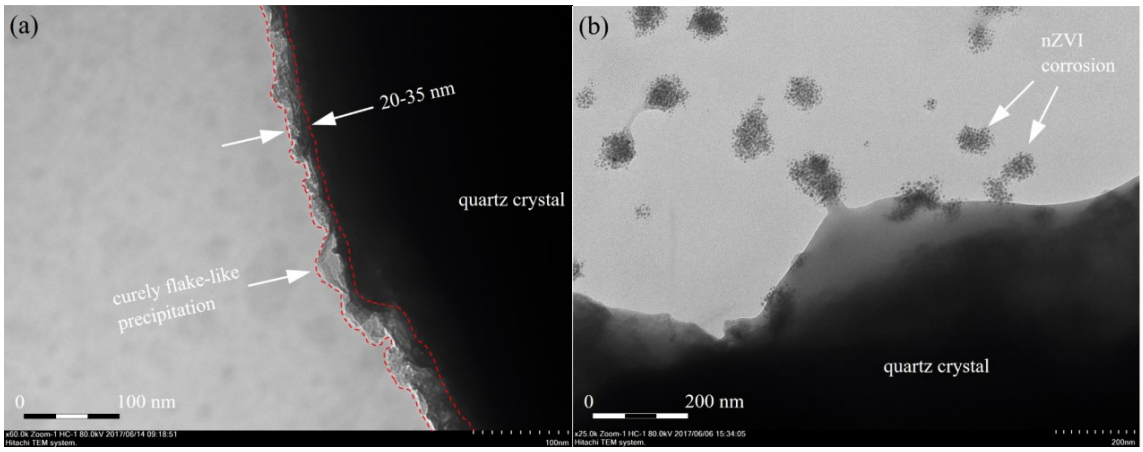

Downloaded by [UNIVERSITY OF WARWICK] on [19/03/19]. Copyright © ICE Publishing, all rights reserved.

Accepted manuscript
doi: 10.1680/jenge.18.00081

Figure 5. Particle size distribution of samples

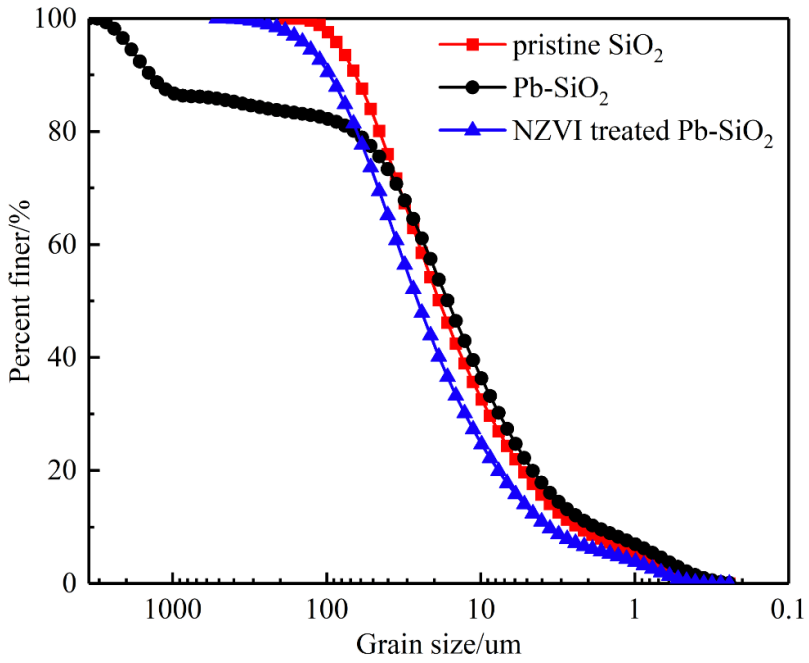

Downloaded by [UNIVERSITY OF WARWICK] on [19/03/19]. Copyright © ICE Publishing, all rights reserved.

Accepted manuscript
doi: 10.1680/jenge.18.00081

Figure 6. The X-ray diffraction (XRD) patterns of each sample: a) pristine SiO_2; b) Pb-SiO_2 (at a Pb-concentration of 400 ppm); c) nZVI treated Pb-SiO_2; d) nZVI-Pb

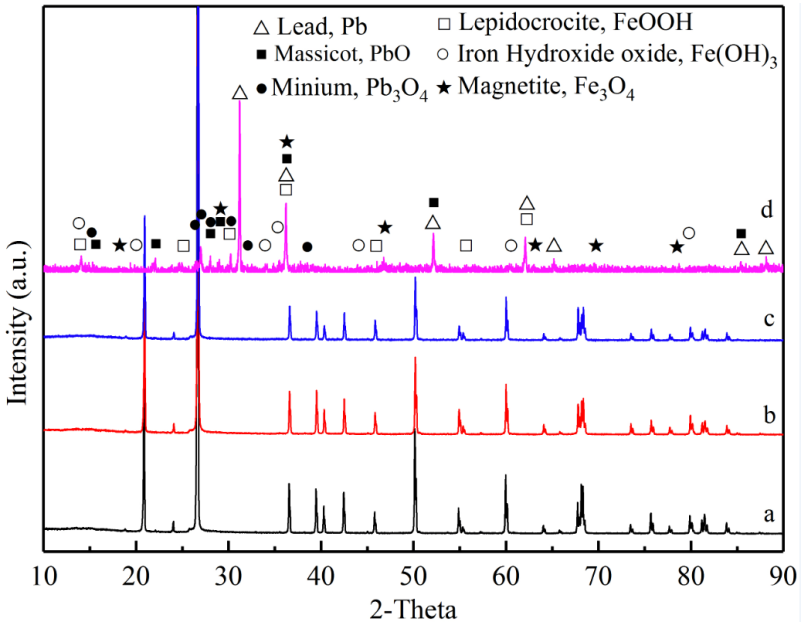

Downloaded by [UNIVERSITY OF WARWICK] on [19/03/19]. Copyright © ICE Publishing, all rights reserved.

Accepted manuscript
doi: 10.1680/jenge.18.00081

Figure 7. Raman spectrum of each sample: a) pristine SiO_2, b) Pb- SiO_2, c) nZVI treated Pb-SiO_2, and d) nZVI-Pb

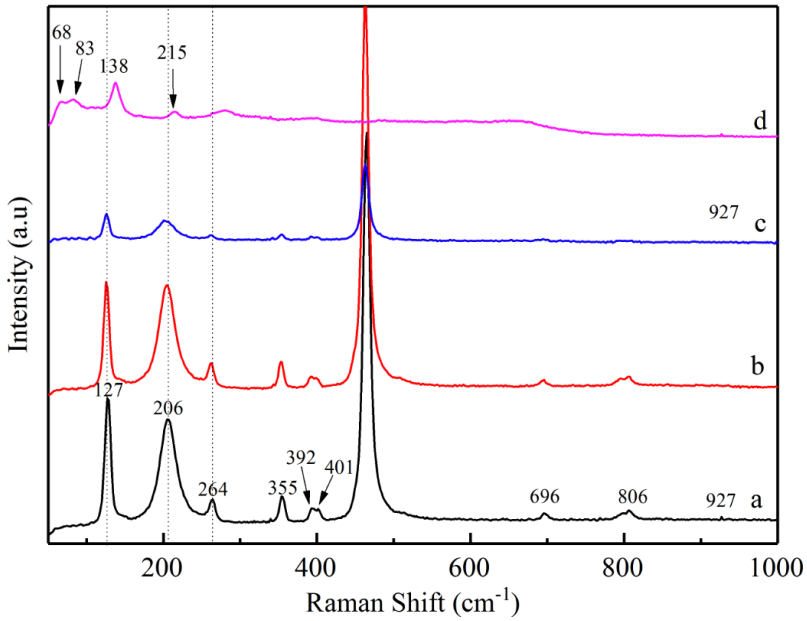

Downloaded by [UNIVERSITY OF WARWICK] on [19/03/19]. Copyright © ICE Publishing, all rights reserved.